

# Scheduling Power-Intensive Operations of Battery Energy Storage Systems and Application to Hybrid Hydropower Plants

Stefano Cassano and Fabrizio Sossan

**Abstract**—Classical schedulers for Battery Energy Storage Systems (BESSs) use static power constraints, assuming that the BESS can provide the rated power at any State-Of-Charge (SOC) level and that these are representative of the underlying physical constraints of the system (BESS voltage and current). Static power constraints, however, can generate unfeasible schedules, especially in power-intensive applications, as demonstrated in this paper. This paper derives a set of alternative constraints for the BESS power that are cognizant of the physical limits of the BESS. It is shown that these constraints, developed by leveraging an equivalent circuit model of the BESS, can be formulated as linear inequalities in scheduling problems, thus leaving the properties of the original problem (i.e., linearity and convexity) unaltered. A comparative analysis against traditional schedulers from the literature shows significant reductions in current violations and the generation of feasible schedules. These findings underscore the crucial role of implementing more advanced power constraints of BESSs in power-intensive applications, thereby enhancing the reliability of BESS scheduling strategies.

**Index Terms**—Scheduler, Battery storage, Optimal control, Hybrid hydropower plants, Frequency regulation.

## I. INTRODUCTION

Applications of Battery Energy Storage Systems (BESSs) are gaining interest in the technical literature and power systems community thanks to maturing electrochemistry and decreasing costs. Advocated BESS applications refer to both behind- and front-of-the-meter contexts and range from energy arbitrage and improvement of PV self-consumption up to grid frequency support, hybridization to improve plants' dynamic performance, and non-wire grid reinforcements.

Operating a BESS normally requires two software layers: a real-time controller and a scheduler.

The real-time controller is responsible for operating the BESS with active and reactive power setpoints that respect the physical limits of the BESS. Physical limits are the current and the voltage on the DC bus and depend on the battery's State Of Charge (SOC). Methods to assess the feasibility of the power setpoints with respect to the DC-bus voltage and current can be categorized into two classes: characteristic maps and model-based approaches. Characteristic maps utilize look-up tables to associate the peak current and power to the battery

SOC, state of health, terminal voltage, and temperature [1]–[3]. Model-based approaches are the SOC-limited [4], voltage-limited ohmic resistance [5], and voltage-limited extrapolation [5], [6] methods.

Schedulers are responsible for ensuring that enough energy is available to provide the prescribed services over time. Schedulers are normally implemented as constrained optimization problems, embedding constraints for the BESS power and SOC. Power constraints, the focus of this paper, are often rendered in the form  $|B| \leq \bar{B}$ , where  $B$  is BESS power and  $\bar{B}$  is the converter kVA rating (e.g., [7], [8]).<sup>1</sup> These “static” constraints are used as a proxy for the underlying BESS current and voltage constraint. Compared to the more detailed physical models used for real-time control described above, they are mathematically tractable in optimization problems because they are linear in the power. However, as shown in Section II of this paper, static power constraints might generate unfeasible schedules, meaning that actuating these schedules could result in violations of the BESS's underlying voltage and current constraints when the BESS is then used in real-time control.

The contribution of this paper to the existing state of the art is twofold. First, in Section III, we propose accurate BESS power constraints derived from a battery equivalent circuit model which are cognizant of the BESS's underlying voltage and current constraints. It is shown that the proposed power constraints can be rendered as a linear function of the BESS historical power, thus leaving the original tractability properties of the scheduling problem (e.g., linearity or convexity) unaltered. Second, the proposed scheduler is applied in Section IV to the problem of scheduling operations of a hybrid hydropower plant. A comparative analysis in Section V shows that the proposed scheduler produces feasible schedules compared to a traditional one.

## II. ON HOW TRADITIONAL SCHEDULERS MIGHT FAIL IN PRODUCING BESS FEASIBLE SCHEDULES

### A. Formulation of the scheduling problem

The objective of a BESS scheduler is to find an appropriate power trajectory to charge or discharge the BESS to ensure that sufficient power and energy levels are available during real-time operations to provide the services for which it is designed. For example, if a battery is nearly fully discharged

<sup>1</sup>Or  $B^2 + Q^2 \leq \bar{B}^2$  if the reactive power is a variable of the scheduling problem [9].

S. Cassano and F. Sossan are with the University of Applied Sciences of Western Switzerland (HES-SO), Switzerland. E-mail: stefano.cassano, fabrizio.sossan@hevs.ch.

Research supported by Innosuisse in the context of the Flagship Project “STORE” (grant agreement 108.230).

but discharging power is needed to provide frequency regulation, the scheduler should intercept this need (typically by implementing forecasts of the service to provide) and recharge the battery preemptively. State-of-the-art BESS schedulers are implemented as a constrained optimization problem, where the cost function represents the operational objective to achieve (e.g., peak shaving, electricity cost optimization, provision of frequency control) and the constraints describe the operational limits of the BESS (e.g., rated power and energy capacity).

A classical formulation of a BESS scheduler from the current state of the art is now presented. Let  $\widehat{B}_t$  be the predicted BESS power (positive when discharging, negative when charging) at time  $t$  in kW. It can be expressed as:

$$\widehat{B}_t = \widehat{P}_t + F_t \quad (1)$$

where  $\widehat{P}_t$  is a point prediction of the power demand of the service to provide (e.g., primary frequency control, peak shaving), and  $F_t$  is a problem slack variable that “releases” the battery from providing the prescribed service if this leads to infeasible conditions. We refer to the sequence  $F_t$  for  $t = 0, \dots, T$  as “offset profile”.

The BESS power should not exceed the power rating of the system. Assuming that the system operates at a unitary power factor, this requirement reads as:

$$-\overline{B} \leq \widehat{B}_t \leq \overline{B}, \quad (2)$$

where  $\overline{B}$  is the kVA rating of the system. The battery SOC in per unit at time  $t + 1$  is approximated with a function of the charging/discharging power  $\widehat{B}_t$  (in kW) with the following explicit equation:

$$SOC_{t+1} = SOC_0 - \frac{\Delta_T}{E^r} \sum_{\tau=0}^t \left( \frac{1}{\eta} [B_\tau]^+ - \eta [B_\tau]^- \right) \quad (3)$$

where  $SOC_0$  is a known initial state of charge,  $\Delta_T$  is the duration in hour of the time interval  $t$ ,  $E^r$  is the BESS rated energy storage capacity in kWh,  $\eta$  is the conversion efficiency, and  $[\cdot]^+$  and  $[\cdot]^-$  denote the positive and negative part of the argument, respectively. For compactness, we denote with the notation  $[x]_{\underline{i}}^{(\overline{i})}$  a vector composed of all the scalars from  $x_{\underline{i}}$  to  $x_{\overline{i}}$ . For example:

$$[\widehat{B}]_0^{(t)} = \left[ \widehat{B}_0 \quad \widehat{B}_1 \quad \dots \quad \widehat{B}_t \right]. \quad (4)$$

By leveraging this notation, Eq. (3) becomes:

$$SOC_{t+1} = SOC_0 - h \left( [\widehat{B}]_0^{(t)} \right), \quad (5)$$

where  $h(\cdot)$  is a scalar-valued function defined as:

$$h \left( [x]_{\underline{i}}^{(\overline{i})} \right) = \frac{\Delta_T}{E^r} \sum_{i=\underline{i}}^{\overline{i}} \left( \frac{1}{\eta} [x_i]^+ - \eta [x_i]^- \right).$$

With these models in place, the BESS scheduling problem can be stated as finding the offset profile  $[F]_0^{(T)}$  so that the constraints on the battery’s power and SOC are respected when the BESS is asked to provide the power  $\widehat{P}_t$  in (1). The scheduler is formulated as the constrained optimization problem (6), where the cost function consists in minimizing

the norm-2 of the offset profile, as a best-effort attempt to provide the required power  $\widehat{P}_t$ , weighted by customizable non-negative coefficients  $c_t$  <sup>(2)</sup>. Its formulation reads as:

$$\arg \min_{[F]_0^{(T)}} \left\{ \sum_{t=1}^T c_t F_t^2 \right\} \quad (6a)$$

subject to:

$$\widehat{B}_t = \widehat{P}_t + F_t, \quad t = 0, 1, \dots, T \quad (6b)$$

$$-\overline{B} \leq \widehat{B}_t \leq \overline{B}, \quad t = 0, 1, \dots, T \quad (6c)$$

$$SOC_{t+1} = SOC_0 - h \left( [\widehat{B}]_0^{(t)} \right), \quad t = 0, 1, \dots, T \quad (6d)$$

$$\underline{SOC} \leq SOC_t \leq \overline{SOC}, \quad t = 1, 2, \dots, T + 1 \quad (6e)$$

The limitations of this formulation are discussed in the next subsection.

### B. Limitations of the above-mentioned formulation

The limitation of the above-mentioned scheduler is that the power constraints in (6c) are, in reality, an approximation of the physical constraints of a battery system. This approximation stems from assuming a constant battery voltage. To explain this proposition, we resort to the equivalent circuit model of a battery shown in Fig. 1. This circuit models the voltage on the battery DC bus, denoted by  $v$ , as a function of the battery discharging current  $i$  (positive when discharging, negative when charging). The circuit consists of two elements: a voltage source  $v_{oc}$  and a series resistance  $R$ , representing the battery’s open circuit voltage and internal resistance, respectively. The values of these two parameters are BESS-specific and can be estimated from measurements.

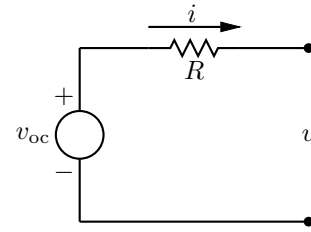


Fig. 1. Steady-state equivalent circuit of the DC bus of a BESS.

In the settings of Fig. 1, the true physical constraints of a BESS concern the voltage level  $v$ , which should stay within an allowed range  $\underline{v}, \overline{v}$ , and the current  $i$ , whose intensity  $|i|$  should remain below a rated value  $\overline{i}$ :

$$\underline{v} \leq v \leq \overline{v} \quad (7)$$

$$-\overline{i} \leq i \leq \overline{i}. \quad (8)$$

It is assumed that the current and voltage constraints of the BESS power converter are less restrictive than those of the battery, so respecting the battery constraint will also respect the converter constraints. In addition, in the spirit of a Thevenin equivalent circuit of the BESS, the ohmic losses of the

<sup>2</sup>Other problem formulations, in particular of the cost function, are possible. This formulation is meant to provide an illustrative example of the limitations of the problem constraints.

converter are assumed to be included in the resistance  $R$  of the DC-bus circuit in Fig. 1.

Assuming that the battery voltage is constant and at the rated value  $v^r$  (with  $\underline{v} \leq v^r \leq \bar{v}$ ) has two implications. First, the battery voltage constraint is respected by construction, so one could ignore this constraint. Second, the current constraint  $-\bar{i} \leq i \leq \bar{i}$  can be equivalently rendered as a power constraint as follows:

$$-\bar{i}v^r \leq iv^r \leq \bar{i}v^r \quad (9a)$$

$$-\bar{p} \leq p \leq \bar{p} \quad (9b)$$

where  $p = iv^r$  is the DC power delivered by the circuit when  $v = v^r$ , and  $\bar{p} = \bar{i}v^r$  is the power at the rated current and rated voltage. In summary, the equations above show that, under the assumption of constant battery voltage, the power constraints become a valid proxy to the current constraints of the battery, justifying its adoption in (6c).

Although the assumption of constant battery voltage might be deemed reasonable in some BESS applications, it generally does not hold, as demonstrated in the next section, leading to unfeasible BESS operations.

### C. Motivating example

The limitations of the BESS scheduler discussed above are now demonstrated with an example. It is considered a BESS with a rated power of  $\bar{B} = 720$  kW and an energy capacity of  $E^r = 560$  kWh. The initial time interval is denoted by  $t = 0$ . The duration of the optimization horizon is  $T = 5$ . The integration time is  $\Delta_t = 5$  minutes. The initial battery state of charge is  $SOC_0 = 20\%$ . At  $t = 2$ , the BESS is called to provide a discharging power of 600 kW for 5 minutes (i.e., 50 kWh); this information is encoded in the vector  $[\hat{B}]_0^{(5)}$ , which is made by all zeros, except for the third element, which is 600 kW. The amount of requested energy corresponds to about 9% of the battery's nominal energy capacity, assuming ideal discharging efficiency. In addition, the battery state-of-charge limits are  $\underline{SOC} = 5\%$  and  $\overline{SOC} = 95\%$ .

For the sake of illustration and before proceeding to the numerical resolution, it is useful to deduce the solution to the scheduling problem by reasoning: the solution of the unconstrained optimization problem associated with (6) is a vector of all zeros, namely  $[F]_0^{(5)} = [0]_0^{(5)}$ ; because this solution does not violate the constraints (6b)-(6c) (indeed, the discharging power of 600 kW required to the battery is smaller than the converter rated power of 720 kW, and the SOC drop of 9% applied to the SOC initial value of 20% is still within the feasible range 5%-95%), one can conclude that the all-zero vector is also solution to the constrained optimization problem in (6).

Resolving the scheduling problem in (6) numerically yields the same solution deduced by reasoning, as shown in the upper panel of Fig. 2.

In Fig. 2, the dashed red lines show the static converter rating (i.e.,  $\pm 720$  kW), referred to as Static Power Constraints (SPCs), whereas the dashed-dotted line in black shows the more accurate power limits calculated by considering the elements previously enounced in II-B and that will be formalized

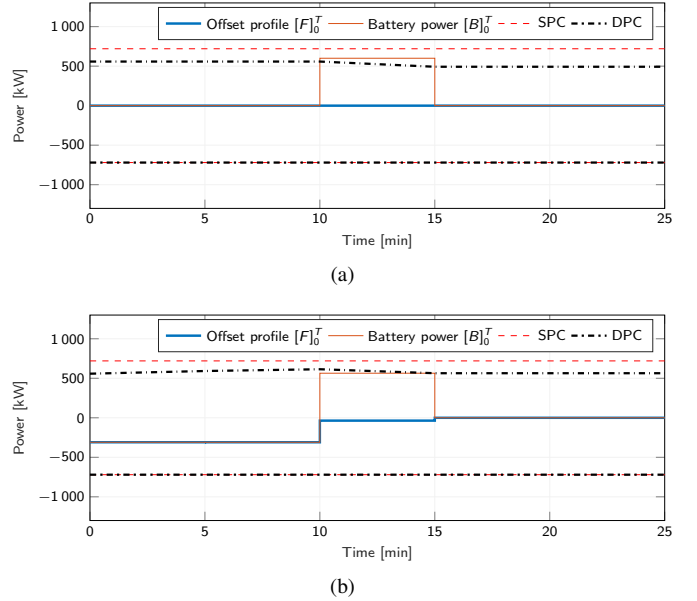


Fig. 2. BESS discharging power and power limits determined by the scheduler under different constraints with Static Power Constraints (SPCs) in (a), and with Dynamic Power Constraints (DPCs) in (b).

in the next section. We refer to this second set of constraints as Dynamic Power Constraints (DPCs).

Fig. 2 (a) shows that the BESS power respects the SPCs, but it exceeds the upper bound of the DPCs. Two elements cause this violation: first, high power requires high current, making under-voltages more likely owing to large voltage drops on the resistance; second, low SOC values result in low open-circuit voltages, causing large current, reinforcing voltage drops and possibly resulting in over-currents. In summary, delivering high discharging power is more prone to over-voltages and over-currents. Because the standard scheduling problem is not informed about voltage and current limits, its solution does not respect the DPCs. The next section shows the formulation of DPCs for the scheduler that is aware of the voltage and current constraints of the BESS' DC bus.

For completeness, Fig. 2 (b) shows the results of applying the scheduler augmented with the proposed constraints: as it can be seen, the BESS discharge limit increases in the first 10 minutes of the scheduling horizon, putting the BESS in a better position to provide the target discharge power of 600 kW. The scheduler achieves this result by preemptively charging the BESS so that it can achieve a higher voltage and respect the constraints.

## III. DYNAMIC POWER CONSTRAINTS FOR THE BESS SCHEDULING PROBLEM

This section describes the central contribution of this paper, which is a formulation for accurate power constraints for BESS scheduling problems that account for the current and voltage physical constraints of the battery.

### A. From voltage and current constraints to power constraints

We are concerned with finding the largest charging (maximum value) and discharging (minimum value) power that a

battery, modeled with the circuit of Fig. 1, can deliver, subject to voltage and current constraints. The battery terminal voltage  $v$  in the circuit in Fig. 1 is given by:

$$v = v_{oc} - Ri. \quad (10)$$

The power  $p$  delivered at the terminal of the circuit is thus:

$$p = vi = (v_{oc} - Ri)i = v_{oc}i - Ri^2. \quad (11)$$

As known from the maximum power transfer theorem, by computing the derivative of (11) with respect to  $i$  and equating it to zero, one can compute the current for which the maximum power transfer occurs. This reads as:

$$\frac{dp}{di} = v_{oc} - 2Ri \quad (12)$$

$$i_{max} = \frac{v_{oc}}{2R}. \quad (13)$$

From (12), it follows that the power  $p$  is a monotonically increasing function of the current  $i$  if  $i < i_{max}$ . Because for real batteries, the battery rated current is typically much smaller than  $i_{max}$ , this condition holds and will be assumed as one operative assumption in the rest of this paper.

As introduced in Section II, the electrical physical constraints of a battery system consist of the battery voltage and current constraints:

$$\underline{v} \leq v \leq \bar{v} \quad (14a)$$

$$-\bar{i} \leq i \leq \bar{i}. \quad (14b)$$

Replacing (10) into (14a) gives:

$$\underline{v} \leq v_{oc} - Ri \leq \bar{v} \quad (15)$$

Rearranging the terms of (15) yields to the following inequalities:

$$\frac{v_{oc} - \bar{v}}{R} \leq i \leq \frac{v_{oc} - \underline{v}}{R}. \quad (16)$$

The left-hand side of the expression above represents, by construction, the lower bound of the current such that the voltage constraints of the battery are respected; the right-hand side is the upper bound.

According to the operative hypothesis stated earlier, the battery power monotonically increases with the current; thus, the current bounds in (16) can be used to find power bounds. In particular, by replacing the current lower and upper bounds of (16) into (11), one can find the power bounds such that the voltage constraints are respected. For the power upper bound, this reads as:

$$\begin{aligned} \bar{p}_v &= v_{oc} \left( \frac{v_{oc} - \underline{v}}{R} \right) - R \left( \frac{v_{oc} - \underline{v}}{R} \right)^2 = \\ &= \frac{\underline{v}}{R} (v_{oc} - \underline{v}). \end{aligned} \quad (17a)$$

For the lower bound, it is:

$$\underline{p}_v = \frac{\bar{v}}{R} (v_{oc} - \bar{v}). \quad (17b)$$

Similarly to the power bounds due to the voltage constraints, one can compute the power bounds due to the current constraints by replacing the lower and upper bounds of (14b) into (11). These power bounds read as:

$$\underline{p}_i = -v_{oc}\bar{i} - R\bar{i}^2 \quad (18a)$$

$$\bar{p}_i = v_{oc}\bar{i} - R\bar{i}^2. \quad (18b)$$

In summary, the initial set of constraints on voltage and current in (14) can be replaced by:

$$p \geq \underline{p} = \max(\underline{p}_v, \underline{p}_i) \quad (19a)$$

$$p \leq \bar{p} = \min(\bar{p}_v, \bar{p}_i). \quad (19b)$$

The advantage of (19) compared to (14) is that, in BESS scheduling problems, the decision variable is normally the battery power and not the battery current and voltage; thus, the virtue of the reformulation in (19) is that explicit constraints on the problem decision variable (i.e., the battery power) can be used to enforce the underlying physical constraints on current and voltage levels.

The rest of this section concerns implementing the constraints (19) in the scheduling problem. The terms  $\underline{p}_v, \underline{p}_i, \bar{p}_v, \bar{p}_i$  on the left-hand side of (19) are as defined in (17) and (18). In order to calculate (17) and (18), one needs the open-circuit voltage  $v_{oc}$ , the voltage limits  $\bar{v}, \underline{v}$ , the rated current  $\bar{i}$  and the series resistance  $R$ . While the rated current, voltage limits and series resistance are constant and known, the open-circuit voltage depends on the battery state of charge, which depends, in turn, on the battery charging/discharging power. Therefore, as shown next, Eq. (19) features an interdependency between the current and past control actions that must be explicitly modeled.

## B. Power constraints as a function of the battery SOC

As known (e.g., [10]–[12]), the open-circuit voltage of a battery depends on its SOC. Fig. 3 shows measurements for the lithium-ion BESS considered in this paper's case study, along with a linear fitting. As visible from the figure, and more generally for lithium-ion technologies, the linear approximation closely resembles the measurements, especially for non-extreme SOC values (e.g., between 5% and 95%). Because during BESS operations, the battery normally operates with some margin from the extreme SOC limits, the linear approximation is considered to hold as accurate in practical applications.

We now use the linear SOC-to-open-circuit-voltage relation of Fig. 3 to calculate the power bounds (17)–(19). The result of this process, which stands as one of the main results of this paper, is shown in Fig. 4: the envelope between the two curves is the feasible operating range of the battery power, and, by construction, it is such that current and voltage constraints are respected. From Fig. 4, one can observe two elements. First, the discharging power monotonically increases with the battery SOC (i.e., the battery can provide more power when fully charged than when discharged), whereas it is vice-versa for the charging power (i.e., at high SOC values, the battery can recharge at a lower rate than when

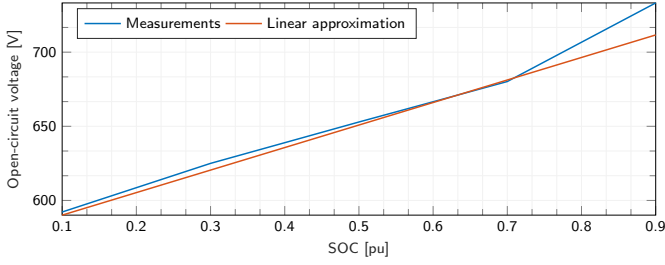


Fig. 3. Open-circuit voltage as a function of the battery state of charge for the lithium-ion BESS considered in this paper's case study.

discharged). Second, the feasible operating area is a convex set. This property is important for the mathematical tractability of the problem because a convex set can be rendered with linear inequalities. We prove in Appendix A that the linear relationship between the battery open-circuit voltage and SOC is a sufficient condition to ensure the convexity of the envelope in Fig. 4.

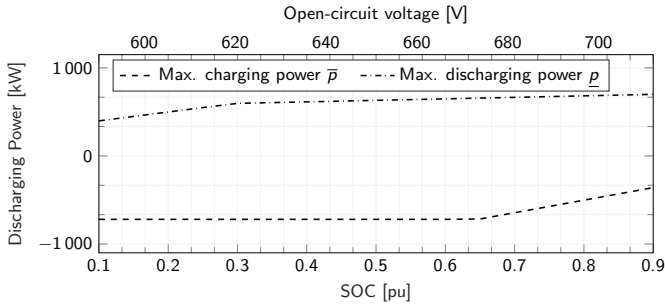


Fig. 4. Feasible power region of the BESS as a function of the battery SOC.

Now that a feasible operating range for the BESS power has been found, it can be included in the scheduling problem, as shown in the next subsection.

### C. Inclusion of power constraints in the scheduling problem

The power capabilities curves of Fig. 4, which denote the feasible operating region for the battery power, are used to replace the static power constraints (6c) in the scheduling problem. We model the upper and lower bounds of the convex envelope of Fig. 4 with the following equations, linear in the variable  $SOC_t$ :

$$\bar{B}_k = \bar{a}_k + \bar{b}_k \cdot SOC_t, \quad k = 1, \dots, K \quad (20a)$$

$$\underline{B}_j = \underline{a}_j + \underline{b}_j \cdot SOC_t \quad j = 1, \dots, J \quad (20b)$$

where  $(\bar{a}_k, \underline{a}_j)$  and  $(\bar{b}_k, \underline{b}_j)$  are coefficients of the linear functions estimated from the curves, and  $K$  and  $J$  are the numbers of linear equations used to approximate the envelope.

By replacing (5) into (20), one can write the BESS power constraints in the following form:

$$B_t \leq \bar{a}_k + \bar{b}_k \cdot \left[ SOC_0 - h \left( [B]_0^{(t-1)} \right) \right], \quad \text{for all } k \quad (21)$$

$$B_t \geq \underline{a}_j + \underline{b}_j \cdot \left[ SOC_0 - h \left( [B]_0^{(t-1)} \right) \right], \quad \text{for all } j \quad (22)$$

which highlights a dependency between the current battery power  $B_t$  and its history  $B_0, B_1, \dots, B_{t-1}$ . Finally, the

scheduling problem presented in (6) can be reformulated as follows:

$$\arg \min_{[F]_0^{(T)}} \left\{ \sum_{t=0}^T f(F_t) \right\} \quad (23a)$$

subject to

$$SOC_{t+1} = SOC_0 - h \left( [B]_0^{(t)} \right) \quad (23b)$$

$$\underline{SOC} \leq SOC_{t+1} \leq \overline{SOC} \quad (23c)$$

for  $t = 0, 1, \dots, T$ , and

$$B_t \leq \bar{a}_k + \bar{b}_k \cdot \left[ SOC_0 - h \left( [B]_0^{(t-1)} \right) \right] \quad (23d)$$

$$B_t \geq \underline{a}_j + \underline{b}_j \cdot \left[ SOC_0 - h \left( [B]_0^{(t-1)} \right) \right] \quad (23e)$$

for  $t = 0, 1, \dots, T$ ,  $k = 1, 2, \dots, K$ , and  $j = 1, 2, \dots, J$ . It is important to remark that if the function  $h_{[t]}(\cdot)$  can be reformulated as a linear function (by way of integer variable or convex relaxations, e.g., [13]), the set of constraints become linear in the battery power  $B_t$ , thus leaving unaltered the original convexity property of the problem. We refer to this set of constraints as DPC.

## IV. APPLICATION: BESS SCHEDULER FOR A HYBRID HYDROPOWER PLANT

This section formulates a BESS scheduler with DPCs to ensure correct operations of the BESS of a hybrid hydropower plant. For the unfamiliar reader, a short preamble explains the notion of hybrid hydropower plants.

### A. Hybrid hydropower plant

A hybrid hydropower plant is a conventional hydropower plant augmented with a BESS installed at the plant's premises. The two units are operated under a unified control framework. The role of the BESS is to take over those power regulation tasks that would engender excess mechanical fatigue on the hydropower plant's mechanical components so as to postpone expensive maintenance and avoid prolonged offline times.

A diagram exemplifying the operational principle of a hybrid hydropower plant is shown in Fig. 5. The power setpoint in the left part of the diagram represents the power requested to the hybrid plant. It comprises components at multiple time scales due to primary frequency control, secondary frequency control, and electricity market commitments. Then, a *power setpoint splitting* procedure shares the power setpoint between the BESS and the hydropower plant; the output of the hybrid plant is finally given by the aggregated contribution of these two units.

The power setpoint splitting procedure is performed by a real-time controller, which computes a decision according to plant conditions and the fatigue-reduction performance to achieve. This work uses the model predictive control (MPC) scheme proposed in [14], [15]. This MPC implements a model-based estimator of the mechanical stress of the hydraulic conduits that detects and removes those patterns of the power setpoint signal that are detrimental to the plant service life.

Other strategies refer to, e.g., low-pass filtering of the control signal.

The contributions of this paper are on the scheduling algorithm and are independent of the specific real-time controller used for the power setpoint splitting and can be applied to other controllers and applications.

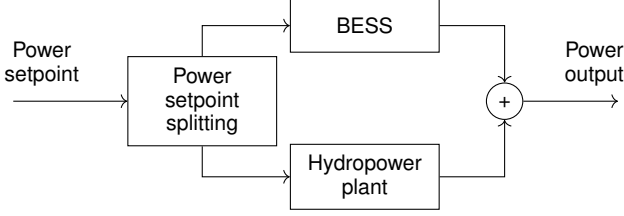


Fig. 5. The power setpoint splitting procedure in a hybrid hydropower plant.

### B. Role of the BESS scheduler

In a hybrid hydropower plant, the role of the BESS scheduler is to ensure that the BESS has sufficient energy reserve to provide the prescribed power services. The relation between the BESS scheduler and the power setpoint splitting problem is shown in Fig. 6: the power setpoint splitting policy operates in real-time (e.g., each 1 second) and computes the BESS. As a result of the actuation of these setpoints, the battery SOC might drift from its original value. In order to compensate for this drift, the scheduler computes a correction to the BESS power (i.e., the offset profile) which is then applied to the real-time control. The scheduler operates at a slower pace than the real-time controller (e.g., every 90 seconds) and in a receding-horizon manner, considering power forecasts of the service that the BESS needs to provide. The formulation of the BESS scheduler is discussed next.

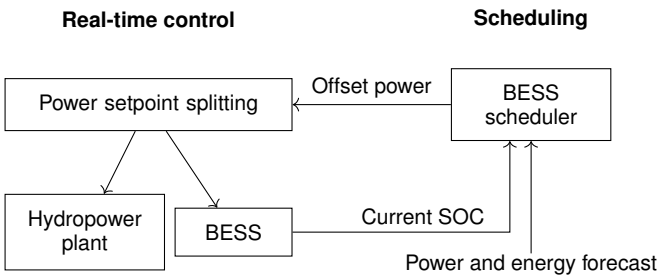


Fig. 6. Signals exchanged between the real-time controller and the BESS scheduler.

### C. Formulation of the BESS constraints for the scheduling problem

This subsection describes three models that are instrumental in formulating the constraints of the scheduling problem: power and energy forecasts to compute the prediction of the battery SOC, the SOC constraints, and the battery power constraints formulated with the method described in Section III.

1) *BESS power and SOC evolution*: As introduced for (1), the BESS power can be modeled as:

$$\widehat{B}_t = \widehat{P}_t + F_t, \quad t = 0, \dots, T-1 \quad (24)$$

where  $\widehat{P}_t$  is a power forecast of the service to provide, and  $F_t$  is offset profile. As the power  $\widehat{P}_t$  of the service to provide might feature large volatility, as for primary frequency control, it is difficult to be forecasted as a point prediction (i.e., the expected value of the realization). For this reason, it is modeled in terms of prediction intervals, which provide a range where the realization is expected to lay with a given confidence level. We denote the lower and upper bound of the prediction interval of  $P_t$  with  $\widehat{P}_t^\downarrow$  and  $\widehat{P}_t^\uparrow$ , respectively, with  $\widehat{P}_t^\downarrow \leq \widehat{P}_t^\uparrow$ . Replacing these forecasts into (24) yield the power bounds for the BESS:

$$\widehat{B}_t^\uparrow = \widehat{P}_t^\uparrow + F_t \quad (25a)$$

$$\widehat{B}_t^\downarrow = \widehat{P}_t^\downarrow + F_t. \quad (25b)$$

By replacing the predictions (25) into the state-of-charge model in (5), one could obtain prediction intervals of the battery SOC under these operating conditions. However, static prediction intervals in the SOC model might lead to unreasonably large energy needs as this entails integrating a constant value over time; in order to avoid large energy needs in the SOC model, we introduce a second set of prediction intervals, called  $\widehat{W}_t^\uparrow, \widehat{W}_t^\downarrow$  (assumed with smaller absolute value than  $\widehat{P}_t^\downarrow, \widehat{P}_t^\uparrow$ ), which refers to the energy forecasts for the service to deliver, and use these in the SOC model to obtain less conservative estimates of SOC needs. To exemplify the situation, let us consider the provision of primary frequency regulation with a droop controller. The power to deliver is proportional to the deviation of the grid frequency from the nominal value (50 Hz), the droop coefficient, and the plant's rated power. This power contribution for primary frequency control might be large; however, it is not sustained for long because, in minutes, secondary frequency control intervenes to re-dispatch generators, releasing the power previously activated for primary frequency control. Thus, being primary frequency control characterized by potentially large power values but modest energy, it is a power-intensive application. Power forecasts  $\widehat{P}_t^\downarrow, \widehat{P}_t^\uparrow$  and energy forecasts  $\widehat{W}_t^\uparrow, \widehat{W}_t^\downarrow$  are designed with the spirit of capturing this property. An example of the computation of these forecasts is given in Section IV-E.

The energy prediction intervals are applied to the model (5) to estimate the prediction intervals of the SOC. This reads as:

$$\widehat{SOC}_{t+1}^\downarrow = SOC_0 - h \left( [\widehat{W}_t^\uparrow + F]_0^{(t)} \right) \quad (26a)$$

$$\widehat{SOC}_{t+1}^\uparrow = SOC_0 - h \left( [\widehat{W}_t^\downarrow + F]_0^{(t)} \right), \quad (26b)$$

for all  $t$ . These estimations will be used in the next paragraph to formulate constraints on the battery SOC.

2) *SOC constraints*: The battery SOC in (26) should remain within (customizable) limits  $\underline{SOC}, \overline{SOC}$ . Because  $\widehat{SOC}_t^\uparrow$  is

larger than  $\widehat{SOC}_t^\downarrow$  by construction, we can apply the upper bound to  $\widehat{SOC}_t^\uparrow$  and the lower bound to  $\widehat{SOC}_t^\downarrow$ :

$$\widehat{SOC}_t^\uparrow \leq \overline{SOC} \quad (27)$$

$$\widehat{SOC}_t^\downarrow \geq \underline{SOC}, \quad (28)$$

for all  $t$ .

3) *BESS power constraints*: We are concerned with ensuring that the BESS expected power, modeled in (25) with prediction intervals, does not exceed the BESS power capabilities, which, as explained in III-C, depend on the battery SOC. Recalling from the previous section, the battery power limits are given by:

$$\overline{B} \leq \overline{a}_k + \overline{b}_k \cdot SOC_t, \quad k = 1, \dots, K \quad (29a)$$

$$\underline{B} \geq \underline{a}_j + \underline{b}_j \cdot SOC_t \quad j = 1, \dots, J \quad (29b)$$

where  $\overline{a}_k$ ,  $\overline{b}_k$ ,  $\underline{a}_j$ , and  $\underline{b}_j$  are given parameters, and  $SOC_t$  is the state of charge at the time interval of interest (which in turn depends on turn on the battery utilization history).

Because  $\widehat{B}_t^\uparrow < \widehat{B}_t^\downarrow$  by construction, one could proceed with applying the larger power limit  $\overline{B}$  to the battery power's upper bound  $\widehat{B}_t^\uparrow$ , and the lower limit  $\underline{B}$  to the battery power's lower bound  $\widehat{B}_t^\downarrow$ , (i.e., two sets of constraints). However, the quantity  $SOC_t$ , required in (29) to compute the bounds, is uncertain as it depends on the battery utilization. This uncertain SOC trajectory was characterized in (26) in terms of prediction intervals with the identification of the upper and lower bound trajectories of the state of charge,  $\widehat{SOC}_t^\uparrow$  and  $\widehat{SOC}_t^\downarrow$ , respectively. Because the trajectory of the SOC realization  $SOC_t$  is likely to lie between  $\widehat{SOC}_t^\uparrow$  and  $\widehat{SOC}_t^\downarrow$ , the battery power limits should be written for both these SOC trajectories in order to ensure that they are respected under any possible realization of the battery power within the identified prediction intervals. This requirement leads to formulating two sets of constraints for the battery's power upper bound (one evolving with  $\widehat{SOC}_t^\uparrow$  and the other with  $\widehat{SOC}_t^\downarrow$ ), and two sets for the battery's power lower bound (i.e., four sets of constraints, in total). Finally, this formulation reads as:

$$\widehat{B}_t^\uparrow \leq \overline{a}_k + \overline{b}_k \cdot \left[ SOC_0 - h \left( [\widehat{W}^\uparrow + F]_0^{(t)} \right) \right] \quad (30a)$$

$$\widehat{B}_t^\uparrow \leq \overline{a}_k + \overline{b}_k \cdot \left[ SOC_0 - h \left( [\widehat{W}^\downarrow + F]_0^{(t)} \right) \right] \quad (30b)$$

$$\widehat{B}_t^\downarrow \geq \underline{a}_j + \underline{b}_j \cdot \left[ SOC_0 - h \left( [\widehat{W}^\downarrow + F]_0^{(t)} \right) \right] \quad (30c)$$

$$\widehat{B}_t^\downarrow \geq \underline{a}_j + \underline{b}_j \cdot \left[ SOC_0 - h \left( [\widehat{W}^\uparrow + F]_0^{(t)} \right) \right]. \quad (30d)$$

#### D. Formulation of the scheduling problem

Consider to be at the time interval  $t = 0$ ; according to the estimation currently delivered by the battery management system, the BESS state-of-charge is  $SOC_0$ . The sequences  $[P]_0^{(T)}$  and  $[W]_0^{(T)}$  store, respectively, the forecasts for peak power utilization and energy utilization for the service that the BESS should deliver (e.g., fatigue reduction service in the hybrid hydropower plant or primary frequency control) over the future time horizon  $t = 0, 1, \dots, T$ .

The BESS scheduling problem computes the sequence  $[F]_0^{(T)}$  so as to ensure that the BESS constraints (state of charge  $SOC_t$  and power  $B_t$  for  $t = 0, \dots, T$ ) will be respected under the BESS utilization forecasts. The formulation reads as the following constrained optimization problem:

$$\arg \min_{[F]_0^{(T)}} \left\{ \sum_{t=0}^T F_t^2 \right\} \quad (31a)$$

subject to the SOC models and constraints

$$SOC_0 - h \left( [\widehat{W}^\uparrow + F]_0^{(t)} \right) \geq \underline{SOC} \quad (31b)$$

$$SOC_0 - h \left( [\widehat{W}^\downarrow + F]_0^{(t)} \right) \leq \overline{SOC} \quad (31c)$$

for  $t = 0, \dots, T$ ; and the battery power limit

$$\widehat{P}_t^\uparrow + F_t \leq \overline{a}_k + \overline{b}_k \cdot \left[ SOC_0 - h \left( [\widehat{W}^\uparrow + F]_0^{(t)} \right) \right] \quad (31d)$$

$$\widehat{P}_t^\uparrow + F_t \leq \overline{a}_k + \overline{b}_k \cdot \left[ SOC_0 - h \left( [\widehat{W}^\downarrow + F]_0^{(t)} \right) \right] \quad (31e)$$

$$\widehat{P}_t^\downarrow + F_t \geq \underline{a}_j + \underline{b}_j \cdot \left[ SOC_0 - h \left( [\widehat{W}^\downarrow + F]_0^{(t)} \right) \right] \quad (31f)$$

$$\widehat{P}_t^\downarrow + F_t \geq \underline{a}_j + \underline{b}_j \cdot \left[ SOC_0 - h \left( [\widehat{W}^\uparrow + F]_0^{(t)} \right) \right], \quad (31g)$$

for  $t = 0, \dots, T$ ,  $k = 1, \dots, K$ , and  $j = 1, \dots, J$ .

The cost function in (31a) is designed to minimize the norm-2 of  $[F]_0^{(t)}$ , which consists of the difference between the battery power output and its forecast (tracking error). The sequence  $[F]_0^{(t)}$  will be of all zeros unless the BESS utilization forecasts will drive the battery out of its constraints.

Compared to the constraint set in (30), the left hand-sides of inequalities (31d)-(31g) have been rendered by using (25) to highlight the dependency of the constraints on the problem variable  $F_t$ .

The optimization problem (31) is applied in a receding horizon manner, i.e., the optimization is repeated periodically each 90 seconds with updated information; at each period, only the first decision action of the sequence  $[F]$  is actuated. The (arbitrary) 90-second period is chosen empirically according to the input time series in order to restore a suitable SOC of the BESS.

As a final note, the formulation (31) features hard constraints. In practice, it is recommended to render these constraints as soft ones by customarily adding slack variables to the problem. This will make it possible for the optimization problem to converge even when the hard constraints are violated, enabling the provision of the prescribed power and services in a best-effort mode with feasible control actions.

#### E. Case study

The simulation case study is a 230 MW medium-head HPP hybridized with a 720 kVA/500 kWh BESS. HPP and BESS characteristics are summarized in Table I.

The simulation model of the hydropower plant is an equivalent circuit model, as in [16]. The model captures hydraulic transients, pressure losses in the pipes, and turbine behavior through the characteristic curves. The synchronous generator torque is modeled with a second-order model, with the electrical torque function of the generator's power angle and



rotor dynamics simulated with the swing equation. The control model used in the MPC is a linear reduced-order model of the simulation model based on [17]. The grid is modeled as an infinite bus, where the rest of the power system imposes the grid frequency under the assumption that its size is significantly larger than the plant. Grid frequency variations in the simulation are reproduced considering real system frequency measurements of the European interconnected system from [18].

TABLE I  
PARAMETERS OF THE SIMULATION CASE STUDY

Parameter	Unit	Value
HYDROPOWER PLANT		
Nominal power	MW	230
Nominal head	m	315
Nominal discharge	m <sup>3</sup> /s	85.3
Nominal speed	rpm	375
Nominal torque	MNm	5.86
Length of penstock	m	1100
Diameter of penstock	m	5
Wave speed	m/s	1100
BATTERY ENERGY STORAGE SYSTEM		
Converter rated power	kVA	750
Nominal energy capacity	kWh	500
Max DC voltage $\bar{v}$	V	750
Min DC voltage $\underline{v}$	V	530
Max DC charging current $-\bar{i}$	A	760
Max DC discharging current $\bar{i}$	A	1350

#### F. Primary and secondary frequency regulation

The plant is equipped with a standard governor consisting of a proportional-integral speed regulator, a speed droop for primary frequency regulation, and a speed changer setting for secondary frequency regulation. The speed regulator's parameters are set to respect pre-qualification tests set by ENTSOE for primary and secondary frequency control [19]. The speed drop is 2%: compared to the conventional higher values (e.g., 5%), 2% is chosen to reproduce future operational settings where the plant is asked to provide higher flexibility. The plant provides two services: primary frequency and secondary frequency regulation. The former quantity is released as a function of the droop coefficient and the grid frequency; the latter is according to the control signal for secondary frequency control shown in Fig. 7, which is from the case study described in [20].

#### G. Forecasting BESS's power and energy needs for fatigue reduction

The scheduling problem requires prediction intervals of the power and energy of the BESS. These prediction intervals are estimated on the basis of historical data of the battery utilization, as described next.

1) *Power prediction intervals*: Given with historical battery power data at a 1-second resolution stored in the sequence  $[P]$ , an empirical probability distribution function is built by

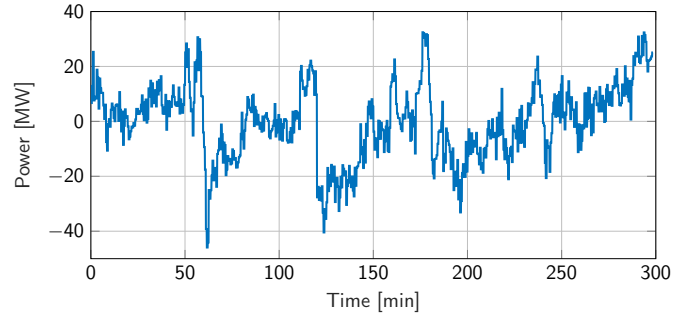


Fig. 7. Power setpoints for secondary frequency control.

computing the histogram of  $[P]$ , shown in the left panel of Fig. 8; prediction intervals are computed by calculating the 5% and 95% percentiles of such a distribution.

2) *Energy prediction intervals*: In order to estimate the energy capacity requirements associated with delivering the power  $[P]$ , the series  $[P]$  is first resampled at a 90 second resolution by sample average and multiplied for the new time resolution to obtain energy values. Then, an empirical distribution of this new series is derived by computing the histogram, shown in the right panel of Fig. 8. Prediction intervals are finally derived by considering the 5% and 95% percentiles of this distribution.

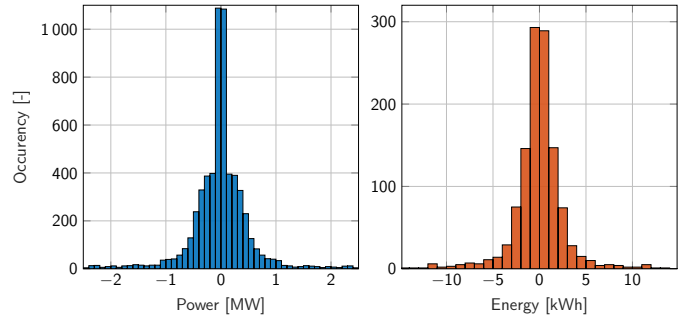


Fig. 8. Empirical distributions of the battery power time series: original series sampled at a 1-second resolution (left), and resampled at a 10-second resolution by sample average (right).

By comparing the histograms in Fig. 8, one can note that while the values of  $[P]$  in the left-panel plot are between  $\pm 2$  MW, the energy values in the right-panel plot feature a remarkably smaller volatility, thus denoting that providing primary frequency control is mainly a power-intensive service.

## V. RESULTS AND DISCUSSION

This section analyses the performance of the DPC scheduler and compares it against the SPC scheduler. The analysis aims to quantify the current violations (which reflect unfeasible operations for the BESS, thus a failure of the scheduling task) that occur during BESS real-time operations when deploying one or the other scheduler. As this section will show, deploying a schedule with DPC achieves fewer and smaller current constraint violations than SPC. The simulation case study is as discussed in Section IV-E; the lower-level control is actuated each second; the scheduler is updated in a receding horizon



fashion every 90 seconds. Control and scheduling setpoints are actuated in the simulation model described in Section IV-E.

Fig. 9 shows the offset profiles with SPC and DPC (upper-panel plot) and the SOC evolution (lower-panel plot), and it will now be explained. In this simulation, the BESS is operated near either the low SOC values or high SOC values to reproduce challenging conditions for the scheduler. This operating condition could reflect, for example, the provision of multiple services in addition to the fatigue reduction service. The power and energy prediction intervals are  $\hat{P}_t^\uparrow = 600$  kW,  $\hat{P}_t^\downarrow = -600$  kW,  $\hat{W}_t^\uparrow = 4.1$  kWh and  $\hat{W}_t^\downarrow = -5.2$  kWh (calculated as described for Fig. 8).

Fig. 9 shows that the DPC schedule features an initial large charging requirement that brings the battery SOC to 40%. This is because, as per forecasts, the battery cannot provide the forecasted discharging power between  $\pm 600$  kW at such a low SOC. At  $t = 12$  h, the battery is requested to provide a charging power of 250 kW for 3 hours and 50 kW for 9 hours by the additional service. The scheduler with DPC generates a positive offset profile to discharge the battery and keep the SOC level around 60%, where the battery can deliver the predicted power. In contrast, the scheduler with SPC produces an offset profile that keeps the SOC within the limits of 5%-95%, as at these levels, the static power constraints allow the predicted power to be delivered.

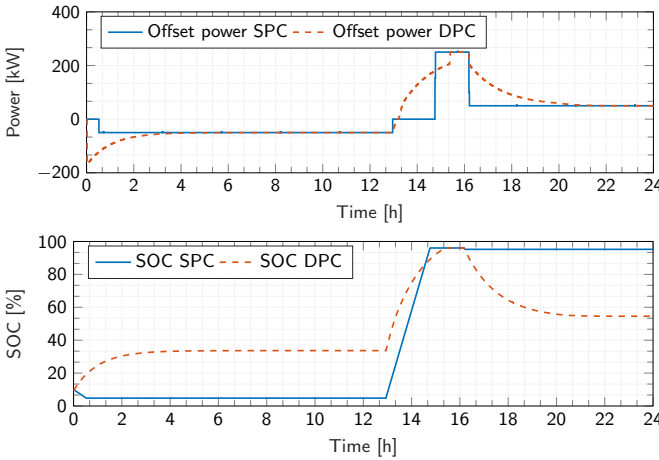


Fig. 9. Offset power  $[F]$  computed by the scheduler with SPC and DPC (top panel) and battery SOC evolution (lower panel).

1) *Assessment of violations of current constraints:* Fig. 10 displays the BESS output current resulting from the two schedulers' actions and the current limits that are a function of the SOC of the battery. The current is retrieved from the BESS power and SOC, leveraging the battery model presented in Fig. 1. In the first 12 hours, the scheduler with DPC charges the battery, increasing the charging current to 960 A. In contrast, the scheduler with SPC maintains a constant SOC of 5%, corresponding to a charging current limit of 520 A. Due to this control action, the number of current limit violations, indicated by the blue and red markers in Fig. 10, is 10 for the scheduler with SPC and 0 for the scheduler with DPC. During the remaining simulation period, the scheduler with DPCs increases the discharging current capability to a value

of -760 A while the scheduler with SPCs maintains the limit of -304 A. This leads the scheduler with SPCs to violate the discharging current limits 19 more times against two times from the scheduler with DPCs. It is worth noting that the scheduler with DPC also exceeds current limits, which is related to the accuracy of the power and energy forecasts.

2) *Performance analysis for different initial SOC levels:*

The analysis has been repeated for different initial SOC levels. For initial SOC between 10 and 50%, it is considered the same additional service and prediction intervals as in the previous analysis, while for SOC between 60% to 90%, the battery must provide a constant discharging power of 50 kW for 12 hours, 250kW of charging power for 3 hours and 50 kW of charging power for the remaining 9 hours. In the latter case, the power predictions remain the same, and the energy predictions are:  $\hat{W}_t^\uparrow = 5.2$  kWh and  $\hat{W}_t^\downarrow = -4.1$  kWh.

The two schedulers have been compared based on the following metrics: the number of current limit violations, the average difference of the current peaks between the upper and lower current limits, and their variance. The results are summarized in Table II. Based on the analysis, the following conclusions can be drawn:

- 1) the scheduler with DPC reduces the number of current violations by 93% in the range 10-50% and by 85% in the range 60-90% of the initial SOC;
- 2) the scheduler with DPC achieves smaller current constraint variations, with a maximum reduction of 60% of the average difference of the current peaks from the limits and a variance lower by two orders of magnitudes.

In conclusion, the results demonstrate that implementing SOC-dependent power constraints in the scheduler's problem formulation considerably impacts the scheduler's performance in power-intensive applications, reducing the probability of producing unfeasible schedules.

TABLE II  
SCHEDULERS' PERFORMANCE COMPARISON ON CURRENT LIMITS VIOLATION.

Type of scheduler	N <sup>o</sup> of violations	Average diff. (upper) [A]	Variance (upper)	Average diff. (lower) [A]	Variance (lower)	Initial SOC [%]
SPC	29	546.63	2.52·10 <sup>3</sup>	-93.51	7.82·10 <sup>3</sup>	10%
DPC	2	-	-	-53.35	13.72	
SPC	28	546.63	2.52·10 <sup>3</sup>	-93.50	7.81·10 <sup>3</sup>	20%
DPC	2	-	-	-53.35	13.72	
SPC	28	546.62	2.52·10 <sup>3</sup>	-93.48	7.81·10 <sup>3</sup>	30%
DPC	2	-	-	-53.35	13.72	
SPC	28	546.62	2.52·10 <sup>3</sup>	-93.48	7.81·10 <sup>3</sup>	40%
DPC	2	-	-	-53.35	13.72	
SPC	28	546.61	2.52·10 <sup>3</sup>	-93.48	7.81·10 <sup>3</sup>	50%
DPC	2	-	-	-53.34	3.86·10 <sup>3</sup>	
SPC	21	335.06	2.06·10 <sup>3</sup>	-83.46	488.26	60%
DPC	3	134.65	43.13	-	-	
SPC	21	335.06	2.06·10 <sup>3</sup>	-83.48	488.26	70%
DPC	3	134.65	43.13	-	-	
SPC	21	335.08	2.06·10 <sup>3</sup>	-83.48	488.27	80%
DPC	3	134.65	43.13	-	-	
SPC	22	335.08	2.07·10 <sup>3</sup>	-83.50	488.27	90%
DPC	3	134.65	43.13	-	-	

## VI. CONCLUSIONS

This paper formulated a new set of BESS power constraints for BESS scheduling problems. It was shown that traditional

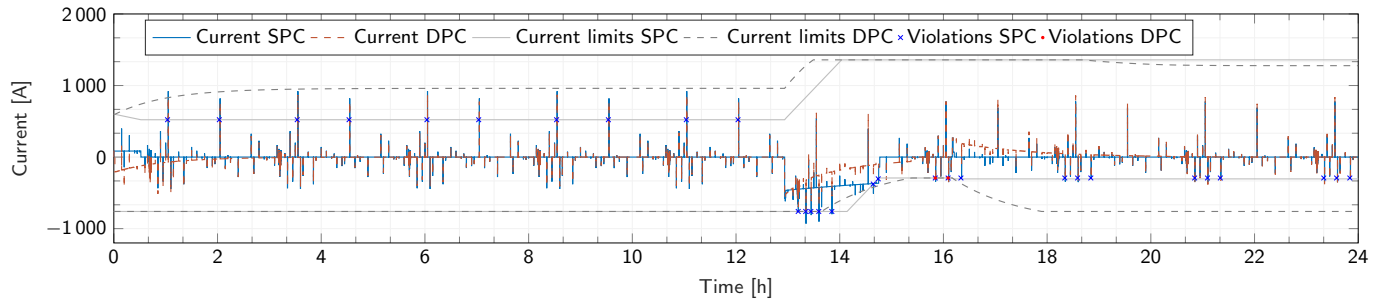


Fig. 10. Battery currents, current limits and violations under the scheduler with static and dynamic power constraints.

schedulers from the literature might fail to produce a reliable schedule because they consider static power constraints of the BESS, i.e., they assume that the BESS can provide the rated power at any level of SOC. To address this shortcoming, we used a model-based approach to derive dynamic capability curves of the BESS power. These curves were successfully integrated into the problem formulation of a scheduler as a set of linear (and convex) power constraints and applied to schedule the operation of a BESS in a hybrid HPP. We compared the traditional scheduler with static power constraints against the proposed one based on (i) the production of a feasible schedule and (ii) the respect of the current limits, under different operating conditions. Results showed that the proposed scheduler performed better in both comparisons. Specifically, it produced a schedule that respected the SOC limitations and significantly reduced the number of current violations by 93% in the SOC range of 10-50% and by 85% in the range of 60-90%. Therefore, implementing SOC-dependent power constraints into the problem formulation of the scheduler is of utmost importance to optimize its efficacy in power-intensive applications.

## APPENDIX A

### CONVEXITY OF THE POWER BOUNDS

**Statement.** *A linear relation between the battery open-circuit voltage and state-of-charge is a sufficient condition to ensure a convex feasible region of the BESS power.*

We denote the epigraph and hypograph of the feasible set in (19) and Fig. 4 by  $g_2$  and  $g_1$ , respectively. For set to be convex,  $g_2$  needs to be convex and  $g_1$  concave. Because the composition of a composition of a convex (concave) function with a linear function preserves convexity (concavity, respectively), the claim is proved.

## REFERENCES

- [1] D. U. Sauer, P. Birke, M. Keller, O. Bohlen, and J. B. Gerschler, "Robust algorithms for a reliable battery diagnosis: managing batteries in hybrid electric vehicles," in *Moving to sustainable mobility: EVS 22, the 22nd International Battery, Hybrid and Fuel Cell Electric Vehicle Symposium and Exposition; proceedings, October 23 - 28, 2006, Yokohama, Japan.*, Tokyo: Japan Automobile Research Institute, 2006.
- [2] X. Liu, Y. Yang, G. Wang, Y. Li, and W. Ma, "Method for estimating the maximum output of a battery for a hybrid electric vehicle," Patent CN101133514B, Dec 16, 2009.
- [3] J. P. Christophersen, "Battery test manual for electric vehicles, revision 3," 6 2015.
- [4] F. Sun, R. Xiong, H. He, W. Li, and J. E. E. Aussems, "Model-based dynamic multi-parameter method for peak power estimation of lithium-ion batteries," *Applied Energy*, vol. 96, pp. 378–386, 2012, smart Grids.
- [5] P. Malysz, J. Ye, R. Gu, H. Yang, and A. Emadi, "Battery state-of-power peak current calculation and verification using an asymmetric parameter equivalent circuit model," *IEEE Transactions on Vehicular Technology*, vol. 65, no. 6, pp. 4512–4522, 2016.
- [6] R. D. Anderson, Y. Zhao, X. Wang, X. G. Yang, and Y. Li, "Real time battery power capability estimation," in *2012 American Control Conference (ACC)*, 2012, pp. 592–597.
- [7] M. Kazemi, H. Zareipour, N. Amjadi, W. D. Rosehart, and M. Ehsan, "Operation scheduling of battery storage systems in joint energy and ancillary services markets," *IEEE Transactions on Sustainable Energy*, vol. 8, no. 4, pp. 1726–1735, 2017.
- [8] M. Elsaadany and M. R. Almassalkhi, "Battery optimization for power systems: Feasibility and optimality," in *2023 62nd IEEE Conference on Decision and Control (CDC)*. IEEE, 2023, pp. 562–569.
- [9] M. Nick, R. Cherkaoui, and M. Paolone, "Optimal allocation of dispersed energy storage systems in active distribution networks for energy balance and grid support," *IEEE Transactions on Power Systems*, vol. 29, no. 5, pp. 2300–2310, 2014.
- [10] F. Sossan, E. Namor, R. Cherkaoui, and M. Paolone, "Achieving the dispatchability of distribution feeders through prosumers data driven forecasting and model predictive control of electrochemical storage," *IEEE Transactions on Sustainable Energy*, vol. 7, no. 4, pp. 1762–1777, 2016.
- [11] F. Berglund, S. Zaferanlouei, M. Korpås, and K. Uhlen, "Optimal operation of battery storage for a subscribed capacity-based power tariff prosumer—a norwegian case study," *Energies*, vol. 12, no. 23, p. 4450, 2019.
- [12] F. Zheng, Y. Xing, J. Jiang, B. Sun, J. Kim, and M. Pecht, "Influence of different open circuit voltage tests on state of charge online estimation for lithium-ion batteries," *Applied energy*, vol. 183, pp. 513–525, 2016.
- [13] M. Kraning, Y. Wang, E. Akuiyibo, and S. Boyd, "Operation and configuration of a storage portfolio via convex optimization," *IFAC Proceedings volumes*, vol. 44, no. 1, pp. 10487–10492, 2011.
- [14] S. Cassano and F. Sossan, "Stress-informed control of medium- and high-head hydropower plants to reduce penstock fatigue," *Sustainable Energy, Grids and Networks*, vol. 31, p. 100688, 2022.
- [15] —, "Model predictive control for a medium-head hydropower plant hybridized with battery energy storage to reduce penstock fatigue," *Electric Power Systems Research*, vol. 213, p. 108545, 2022.
- [16] C. Nicolet, "Hydroacoustic modelling and numerical simulation of unsteady operation of hydroelectric systems," Ph.D. dissertation, EPFL, Lausanne, 2007.
- [17] S. Cassano, F. Sossan, C. Landry, and C. Nicolet, "Performance assessment of linear models of hydropower plants," in *2021 IEEE PES Innovative Smart Grid Technologies Europe (ISGT Europe)*. IEEE, 2021, pp. 01–06.
- [18] M. Pignati, M. Popovic, S. Barreto, R. Cherkaoui, G. D. Flores, J.-Y. Le Boudec, M. Mohiuddin, M. Paolone, P. Romano, S. Sarri *et al.*, "Real-time state estimation of the epfl-campus medium-voltage grid by using pmus," in *2015 IEEE Power & Energy Society Innovative Smart Grid Technologies Conference (ISGT)*. IEEE, 2015.
- [19] ENTSO-E, Ed., "ENTSO-E Statistical Factsheet 2018", Brussels, 2019.
- [20] C. Nicolet, R. Berthod, N. Ruchonnet, and F. Avellan, "Evaluation of possible penstock fatigue resulting from secondary control for the grid," *Proceedings of HYDRO*, 2010.